

General and Localized Corrosion of Outer Barrier of High-Level Waste Container in Yucca Mountain

J. Farmer, D. McCright, G. Gdowski, F. Wang, T. Summers,
P. Bedrossian, J. Horn, T. Lian, J. Estill, A. Lingenfelter, W. Halsey

U.S. Department of Energy

Lawrence
Livermore
National
Laboratory

This article was submitted to
*2000 American Society of Mechanical Engineers, Pressure Vessels
& Piping Conference, Seattle, WA, July 23-27, 2000*

May 2, 2000

DISCLAIMER

This document was prepared as an account of work sponsored by an agency of the United States Government. Neither the United States Government nor the University of California nor any of their employees, makes any warranty, express or implied, or assumes any legal liability or responsibility for the accuracy, completeness, or usefulness of any information, apparatus, product, or process disclosed, or represents that its use would not infringe privately owned rights. Reference herein to any specific commercial product, process, or service by trade name, trademark, manufacturer, or otherwise, does not necessarily constitute or imply its endorsement, recommendation, or favoring by the United States Government or the University of California. The views and opinions of authors expressed herein do not necessarily state or reflect those of the United States Government or the University of California, and shall not be used for advertising or product endorsement purposes.

This is a preprint of a paper intended for publication in a journal or proceedings. Since changes may be made before publication, this preprint is made available with the understanding that it will not be cited or reproduced without the permission of the author.

This report has been reproduced
directly from the best available copy.

Available to DOE and DOE contractors from the
Office of Scientific and Technical Information
P.O. Box 62, Oak Ridge, TN 37831
Prices available from (423) 576-8401
<http://apollo.osti.gov/bridge/>

Available to the public from the
National Technical Information Service
U.S. Department of Commerce
5285 Port Royal Rd.,
Springfield, VA 22161
<http://www.ntis.gov/>

OR

Lawrence Livermore National Laboratory
Technical Information Department's Digital Library
<http://www.llnl.gov/tid/Library.html>

GENERAL AND LOCALIZED CORROSION OF OUTER BARRIER OF HIGH-LEVEL WASTE CONTAINER IN YUCCA MOUNTAIN

**Joseph Farmer, Daniel McCright, Gregory Gdowski, Francis Wang, Tammy Summers,
Peter Bedrossian, Joann Horn, Tiangan Lian, John Estill, Al Lingenfelter & William Halsey**
Yucca Mountain Project
Lawrence Livermore National Laboratory
Livermore, California

INTRODUCTION

As described in the License Application Design Selection Report, the recommended waste package design is Engineering Design Alternative II (CRWMS M&O 1999). This design includes a double-wall waste package (WP) underneath a protective drip shield (DS). The purpose and scope of the process-level model described here is to account for both general and localized corrosion of the waste package outer barrier (WPOB), which is assumed to be Alloy 22 (UNS N06022-21Cr-13Mo-4Fe-3W-2C-Ni (ASTM 1997a). This model will include several sub-models, which will account for dry oxidation (DOX), humid air corrosion (HAC), general corrosion (GC) in the aqueous phase, and localized corrosion (LC) in the aqueous phase. This model serves as a feed to the waste package degradation (WAPDEG) code for performance assessment.

Waste Package Outer Barrier. Alloy 22 (UNS N06022) is now being considered for construction of the outer barrier of the WP. This alloy consists of 20.0-22.5% Cr, 12.5-14.5% Mo, 2.0-6.0% Fe, 2.5-3.5% W, 2.5% (max.) C, and balance Ni (ASTM 1997a). Other impurity elements include P, Si, S, Mn, Co, and V (Treseder et al. 1991). Alloy 22 is less susceptible to LC in environments that contain Cl⁻ than Alloys 825 and 625, materials of choice in earlier designs. The unusual LC resistance of Alloy 22 is apparently due to the additions of Mo and W, both of which are believed to stabilize the passive film at very low pH (Hack 1983). The oxides of these elements are very insoluble at low pH. Consequently, Alloy 22 exhibits relatively high thresholds for localized attack. Very high repassivation potentials have been observed by some (Gruss et al. 1998), while others have found very low corrosion rates in simulated crevice solutions containing 10 wt. % FeCl₃ (Gdowski 1991; Haynes 1987, 1988). Furthermore, no significant localized attack of Alloy 22 has been seen in crevices exposed to water compositions

representative of those expected in the repository. Such tests have been conducted in the Yucca Mountain Project's (YMP's) Long Term Corrosion Test Facility (LTCTF) (Estill 1998). Test media used in this facility include simulated acidic concentrated water (SAW), which is about one-thousand times more concentrated than the ground water at Yucca Mountain (J-13 well water) and which has been acidified with H₂SO₄ (Gdowski 1997c). The measured pH of SAW is approximately 2.7.

Surface Environment. The WP will experience a wide range of conditions during its service life. Initially, the high-level waste containers will be hot and dry due to the heat generated by radioactive decay. However, the temperature will eventually drop to levels where both HAC and aqueous phase corrosion (APC) will be possible. Crevices will be formed between the WP and supports, beneath mineral precipitates, corrosion products, dust, rocks, cement, and biofilms, and between layers of the containers. There has been concern that the crevice environment may be more severe than the near field environment (NFE). The hydrolysis of dissolved metal can lead to the accumulation of H⁺ and a corresponding decrease in pH. Electromigration of Cl⁻ (and other anions) into the crevice must occur to balance cationic charge associated with H⁺ ions (Gartland 1997; Walton et al. 1996). These exacerbated conditions can set the stage for subsequent attack of the corrosion resistant material by passive corrosion, pitting (initiation and propagation), stress corrosion cracking (SCC), or other mechanisms.

Integrated Corrosion Model. The model for the general and localized corrosion of Alloy 22 is summarized in Figures 1 and 2. The threshold relative humidity (RH) is first used to determine whether or not DOX will take place. If DOX is determined to occur, the parabolic growth law represented by Equations 1 and 2 is then used to calculate the corrosion rate as a function of temperature. If the threshold RH is exceeded, HAC will occur in the absence

of dripping water, and APC will occur in the presence of dripping water. If APC is assumed to occur, the corrosion and critical potentials are used to determine whether the mode of attack is general or localized. Correlations can be used as the basis for estimating these potentials at the 50th percentile. Since the material specifications can be based partly on the measured corrosion and threshold (critical) potentials, it can be assumed that these potentials will be uniformly distributed about the 50th percentile values determined from the correlation. For example, the 0th and 100th percentile values of E_{corr} can be assumed to be at E_{corr} (50th percentile) \pm 75 mV. Similarly, the 0th and 100th percentile values of $E_{critical}$ can be assumed to be at $E_{critical}$ (50th percentile) \pm 75 mV. In principle, material falling outside of these specified ranges would not be accepted. Other equivalent correlations of E_{corr} and $E_{critical}$ based upon data relevant to the repository, can also be used. If the comparison of E_{corr} to $E_{critical}$ indicates GC, the distribution of rates determined from the LTCTF will be used as the basis of the GC rate. A study of four test coupons of Alloy 22 removed from the LTCTF after one year showed varying degrees of coverage by silicate deposits but no evidence of localized corrosion by pitting. If the comparison indicates localized corrosion, the distribution of rates presented in Figure 6 will be used. This distribution can be corrected for the maximum bias due to SiO₂ deposit formation by adding a constant value of 63 nm y⁻¹ to each estimated value of the GC rate. This is equivalent to shifting the curve shown in Figure 6 to the right by 63 nm y⁻¹. Corrosion rates will be enhanced to account for MIC above 90% RH. The effect of thermal aging on the corrosion rate is accounted for in the enhancement factor, G_{aged} and is based upon a ratio of the non-equilibrium current densities for base metal and aged material. The value of G_{aged} for base metal is approximately one ($G_{aged} \sim 1$), whereas the value of G_{aged} for fully aged material is larger ($G_{aged} \sim 2.5$). Material with less precipitation than the fully aged material would have an intermediate value of G_{aged} ($1 \leq G_{aged} \leq 2.5$).

DRY OXIDATION

Dry oxidation (DOX) of Alloy 22 is assumed to occur at any $RH < RH_{critical}$, thereby forming an adherent, protective oxide film of uniform thickness. The concept of threshold RH is discussed in greater detail in the following section. It is assumed that the protective oxide film is primarily Cr₂O₃. The rate of DOX is assumed to be limited by mass transport through this growing metal oxide film. Fick's first law is applied, assuming a linear concentration gradient across the oxide film of thickness x . Integration shows that the oxide thickness should obey the following parabolic growth law, also known as Wagner's Law (Welsch et al. 1996), where the film thickness is proportional to the square root of time. This is represented by Equation 1.

$$x = \sqrt{x_0^2 + k \times t} \quad (\text{Eq. 1})$$

where x_0 is the initial oxide thickness, x is the oxide thickness at time t , and k is a temperature-dependent parabolic rate constant.

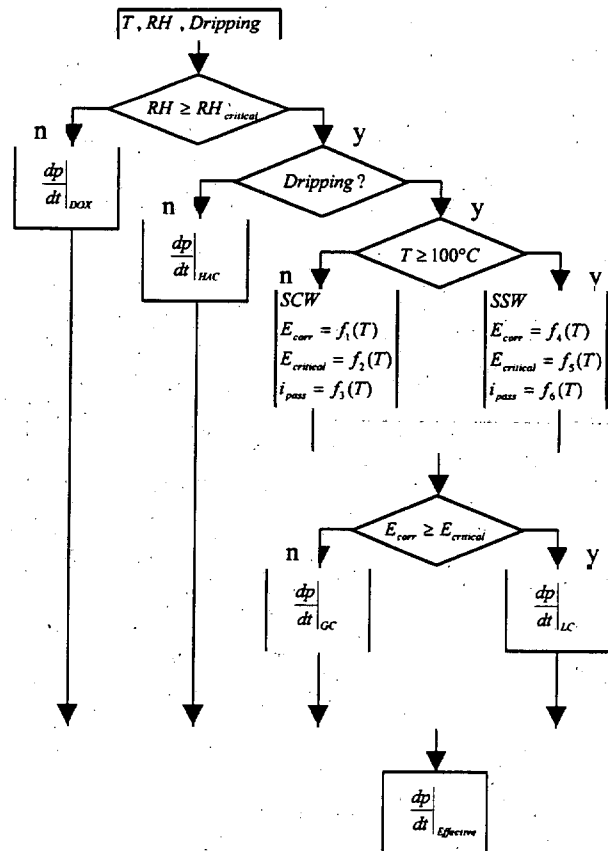


Figure 1. Schematic Representation of Corrosion Model for Alloy 22 Outer Barrier

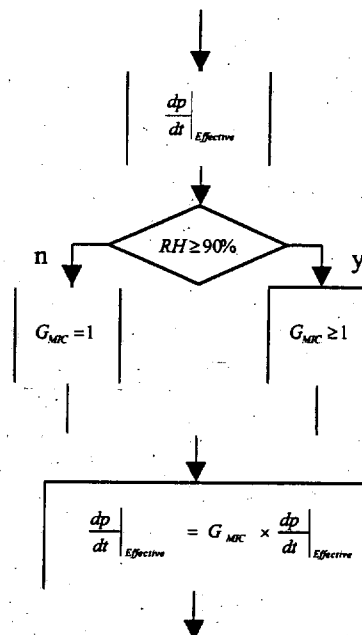


Figure 2. Schematic Representation Showing Augmentation of Model to Account for MIC (or Aging)

The rate constant in Equation 1 is defined as follows:

$$\log[k(m^2 s^{-1})] = -12.5 \left(\frac{10^3}{T(K)} \right) - 3.5 \quad (\text{Eq. 2})$$

where T is defined as the absolute temperature. The highest temperature is expected to be approximately 350°C (623 K), which corresponds to the limit for the fuel cladding. The value of k corresponding to this upper limit is $2.73 \times 10^{-24} \text{ m}^2 \text{ s}^{-1}$ (8.61×10^{-5} square μm per year). After one year, this corresponds to a growth of 0.0093 μm (about 9.3 nm y^{-1}). As will be seen in a subsequent discussion, this estimated rate is comparable to that expected for APC at lower temperatures. It is, therefore, assumed that DOX of the Alloy 22 can be accounted for through application of the parabolic law. The above expression represents a conservative upper bound, based upon published data.

The logarithmic growth law may be more appropriate for use at low temperature than the parabolic law. However, such a logarithmic expression predicts that the oxide thickness (penetration) will asymptotically approach a small maximum level. In contrast, the parabolic law predicts continuous growth of the oxide, which is much more conservative. Since such conservative estimates of the rate of DOX do not appear to be life limiting and since reliable data for determining the maximum oxide thickness for Alloy 22 do not appear to be available, the parabolic growth law will be used for the WPOB.

The DOX model presented here assumes uniform oxidation of the WPOB surface. In the future, the possibility of preferential DOX along grain boundaries in the Alloy 22 should be considered. Such preferential attack would ultimately be diffusion controlled, with the diffusion path being equivalent to the length of oxidized grain boundary.

HUMID AIR CORROSION

Humid air corrosion (HAC) is assumed to occur above a threshold RH, provided that there are no impinging drips.

$$RH \geq RH_{critical} \quad (\text{Eq. 3})$$

This threshold RH for HAC ($RH_{critical}$) is assumed to obey Equation 4. The existence of this threshold is due to the dependence of water adsorption on RH.

As discussed by Gdowski (2000), hygroscopic salts may be deposited by aerosols and dust introduced with the backfill and ventilation air. They will be contained in seepage water that enters the drifts and the episodic water that flows through the drifts. Such hygroscopic salts enable aqueous solutions to exist as thin surface films at relative humidities below 100%. The threshold RH ($RH_{critical}$) at which an aqueous solution can exist is defined as the deliquescence point by Gdowski (2000). This threshold defines the condition necessary at a given temperature for aqueous-phase electrochemical corrosion reactions between a metal substrate and a salt deposit. The deliquescence point of NaCl is relatively constant with temperature, and varies from 72-75%. In contrast, the deliquescence point of NaNO_3 has a strong dependence on temperature, ranging

from an RH of 75.36% at 20°C to 65% at 90°C. The implied equilibrium RH is 50.1% at 120.6°C, the boiling point of a saturated NaNO_3 solution at sea level. The primary uncertainty in the threshold RH for HAC and APC is due to the presence of nitrate. Values of the equilibrium RH for a saturated solution of NaNO_3 are given by Gdowski (2000). It is assumed that any other salts with lower deliquescence points ($RH_{critical}$) are precipitated in surrounding rock before they reach the WP surface. For the time being, this threshold is assumed to obey the following polynomial in temperature, which is a fit of the data deliquescence point data for NaNO_3 :

$$RH_{critical} = -3.5932 \times 10^{-5} \times T(^{\circ}\text{C})^3 + 5.9649 \times 10^{-3} \times T(^{\circ}\text{C})^2 - 0.45377 \times T(^{\circ}\text{C}) + 81.701 \quad R^2 = 0.9854$$

(Eq. 4)

where R^2 is the coefficient of determination and where R is the coefficient of correlation. This correlation is compared to the data in Figure 3.

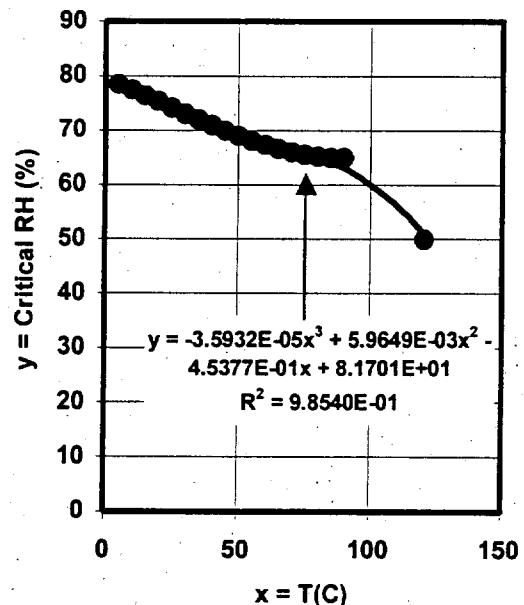


Figure 3. Deliquescence Point for NaNO_3 Solution – Basis for the Threshold Relative Humidity at the 50th Percentile

As pointed out by Gdowski (2000), observed deliquescence points cover a very broad range of RH. For example, the deliquescence point of NaOH is 1.63% RH at 75°C, while that of K_2SO_4 is 97.59% RH at 20°C. It is assumed that the uncertainty in $RH_{critical}$ can be represented by a triangular distribution. The value at the 50th percentile is represented by Equation 4. Values at the 0th and 100th percentiles are assumed to be 1.63 and 97.59%, respectively. The specified bounds represent possible binary combinations of anions and cations in J-13 well water.

Data published by Leygraf (1995) indicates that it may be reasonable to consider HAC at a RH below that predicted with Equation 4 at 20°C. The approximate number of water monolayers on a typical metal surface as a function of RH is given by Leygraf (1995) and repeated in Table 1.

Table 1. Coverage of Metal Surfaces by Water

Relative Humidity (%)	Number of Water Monolayers
20	1
40	1.5-2
60	2-5
80	5-10

Based upon this data, it might be reasonable to consider the possibility of HAC at only 40% RH. This is the point at which it may be possible for two monolayers of water to exist on the WP surface. However, under these conditions there are no electrolytes to facilitate the electrochemical corrosion. The criterion based upon the deliquescence point is believed to be the most defensible.

Aqueous Phase Corrosion

Criterion for Existence of Aqueous Phase. At a given surface temperature, the existence of liquid-phase water on the WP depends upon the presence of a salt deposit. In the presence of such a deposit, a thin-film liquid phase can be established at a higher temperature and lower RH than otherwise possible. In the model discussed here, it is assumed that two conditions must be met for APC — RH above the deliquescence point of the deposit at the temperature of the WP surface (same threshold RH as used for HAC) and impinging drips.

Salt Concentration. As discussed by Gdowski (1997a, 1997b, 1997c), the evaporative concentration of J-13 water results in the concentration of Na^+ , K^+ , Cl^- , NO_3^- , and other ions. Well J-13 water has a typical water chemistry for saturated zone and perched waters at Yucca Mountain and a mean composition that was reported by Harrar et al. (1990). During evaporative concentration HCO_3^- , Ca^{2+} and Mg^{2+} are removed from solution due to carbonate precipitation. The concentration of HCO_3^- reaches a constant level, while the concentrations of F^- and SO_4^{2-} initially increase but eventually fall due to precipitation. Ultimately, the F^- reaches a low steady state value.

Relevant test environments are assumed to include simulated dilute water (SDW), simulated concentrated water (SCW), and simulated acidified water (SAW) at 30, 60, and 90°C, as well as simulated saturated water (SSW) at 100 and 120°C. The SSW used for testing is an abstract embodiment of this observation. The SSW formulation is based upon the assumption that evaporation of J-13 eventually leads to a sodium-potassium-chloride-nitrate solution. The absence of sulfate and carbonate in this test medium is believed to be conservative, in that carbonate would help buffer pH in any occluded geometry such as a crevice. It is well known that polyprotic acids serve as buffers. The compositions of these environments are given in Table 2.

Recently, another relevant test environment has been postulated. Basic Saturated Water (BSW) has a pH between 11 and 13, and a boiling point near 110°C. This test medium was established on the basis of results from a distillation experiment (Wang 1999). The total concentration of dissolved salts in the starting liquid was approximately five-times (5×) more concentrated than that in the standard SCW solution. It was prepared by using five-times the amount of each chemical that is specified for the preparation of SCW. After evaporation of approximately ninety percent (~90%) of the water from the starting solution, the residual solution reaches a maximum chloride concentration and has a boiling point of ~111°C. The resultant BSW solution contains (sampled at 111°C) 9% chloride, 9% nitrate, 0.6% sulfate, 0.1% fluoride, 0.1% metasilicate, 1% TIC (total inorganic carbon from carbonate and bicarbonate), 5% potassium ion and 11% sodium ion. A recipe for preparing synthetic BSW with a pH~11 is shown in Table 3.

The synthetic BSW solution represented by Table 3 has been slightly modified for these and other corrosion tests, yielding BSW-13, BSW-12, and BSW-11. The three solutions have pH values of approximately 13, 12, and 11 respectively. All BSW-type solutions contain 9% chloride, 9% nitrate, 0.6% sulfate, and 0.1% fluoride. Sodium and potassium ions are used to balance the charge. More specifically, each testing solution contains 8.7 g KCl, 7.9 g NaCl, 0.2 g NaF, 13.6 g NaNO_3 , and 1.4 g Na_2SO_4 (anhydrous). The pH 13 solution (BSW-13) was prepared by adding 65 mL of water and 2.0 mL of the 10 N NaOH to the chemicals (total weight = 100 g). The measured pH was 13.13. The pH 12 solution (BSW-12) was prepared by adding 66 mL of water and 2.0 mL of the 1 N NaOH to the chemicals. The measured pH was 12.25. The pH 11 solution (BSW-11) was prepared by adding 66 mL of water and 2.0 mL of the 0.1 N NaOH to the chemicals. The measured pH was 11.11. These recipes are summarized below in Table 4. It should be pointed that the modified BSW solutions are not buffered. In order to add some soluble silica to the solution, the BSW solution recipe was later revised to contain 4.0 g (~1% metasilicate) by adding sodium metasilicate ($\text{Na}_2\text{SiO}_3 \cdot 9\text{H}_2\text{O}$). With the addition of the metasilicate the pH was increased from 11.3 to 13 as measured at room temperature.

It has been noted that the pH of aqueous solutions is dependent on the partial pressure of gaseous CO_2 . The implication of this is that unless many constraints are taken to control the pH of the BSW solution, the pH may vary with test conditions. The partial pressure of CO_2 that is in equilibrium with the revised BSW solution is unknown. In order to conduct a long-term test (few months to a year), the test environment should be stable. It was decided that to make a stable test solution, carbonate and silicates should not be added since both species can affect solution pH. Sodium hydroxide is used instead to maintain higher pH values. Gaseous CO_2 must be removed from the air passing above the solution since it affects the solution pH. With no gaseous CO_2 in contact with the solution, and no carbonate/bicarbonate and silicates in solution, the test environment is relatively stable.

*American Society of Mechanical Engineers
Seattle, Washington – July 2000*

Table 2. Composition of Standard Test Media Based Upon J-13 Well Water

Ion	SDW (mg/L ⁻¹)	SCW (mg/L ⁻¹)	SAW (mg/L ⁻¹)	SSW (mg/L ⁻¹)
K ⁺	3.400E+01	3.400E+03	3.400E+03	1.416E+05
Na ⁺	4.090E+02	4.090E+04	3.769E+04	4.870E+05
Mg ⁺²	1.000E+00	1.000E+00	1.000E+03	0.000E+00
Ca ⁺²	5.000E-01	1.000E+00	1.000E+03	0.000E+00
F ⁻	1.400E+01	1.400E+03	0.000E+00	0.000E+00
Cl ⁻	6.700E+01	6.700E+03	2.425E+04	1.284E+05
NO ₃ ⁻	6.400E+01	6.400E+03	2.300E+04	1.310E+06
SO ₄ ⁻²	1.670E+02	1.670E+04	3.860E+04	0.000E+00
HCO ₃ ⁻	9.470E+02	7.000E+04	0.000E+00	0.000E+00
Si	27 (60°C), 49 (90°C)	27 (60°C), 49 (90°C)	27 (60°C), 49 (90°C)	0.000E+00
pH	8.100E+00	8.100E+00	2.700E+00	7.000E+00

Table 3. Initial BSW Solution Recipe

Chemical	Quantity (g)
Na ₂ CO ₃ (anhydrous)	10.6
KCl	9.7
NaCl	8.8
NaF	0.2
NaNO ₃	13.6
Na ₂ SO ₄ (anhydrous)	1.4
H ₂ O	55.7
pH	11.3 (measured at room temperature)

Table 4. Modified BSW Solution Recipes

	BSW-13	BSW-12	BSW-11
Chemical	Quantity	Quantity (g)	Quantity (g)
KCl	8.7 g	8.7 g	8.7 g
NaCl	7.9 g	7.9 g	7.9 g
NaF	0.2 g	0.2 g	0.2 g
NaNO ₃	13.0 g	13.0 g	13.0 g
Na ₂ SO ₄ (anhydrous)	1.4 g	1.4 g	1.4 g
H ₂ O (deionized)	66 ml	66 ml	66 ml
10N NaOH	2 ml		
1N NaOH		2 ml	
0.1N NaOH			2 ml
CO ₂ partial pressure	0	0	0
pH (at room temperature)	13.13	12.25	11.11

Note: The CO₂ partial pressure can be minimized by either scrubbing laboratory air or purchasing CO₂ free air.

Concentration of Dissolved Oxygen. Corrosion rates in the LTCTF may depend upon the concentration of dissolved oxygen because the cathodic reduction of oxygen may be required to depolarize anodic dissolution reactions. The anodic dissolution of a metal requires a corresponding amount of cathodic reduction. Typically, dissolved oxygen or hydrogen ion is reduced. However, other reactants such as hydrogen peroxide (due to gamma radiolysis) can also be reduced. Figure 4 shows a comparison of dissolved oxygen measurements in LTCTF to published data for synthetic geothermal brine (Cramer 1974). The published data spans the range of temperature from 20 to 300°C, and spans the range of oxygen partial pressures from 1 to 30 psi. Note that the partial pressure of oxygen in the atmosphere is about 3 psi. The points representing measurements from the LTCTF tanks are superimposed upon the published data. Clearly, the SDW, SCW, and SAW appear to be saturated (4-10 ppm dissolved oxygen).

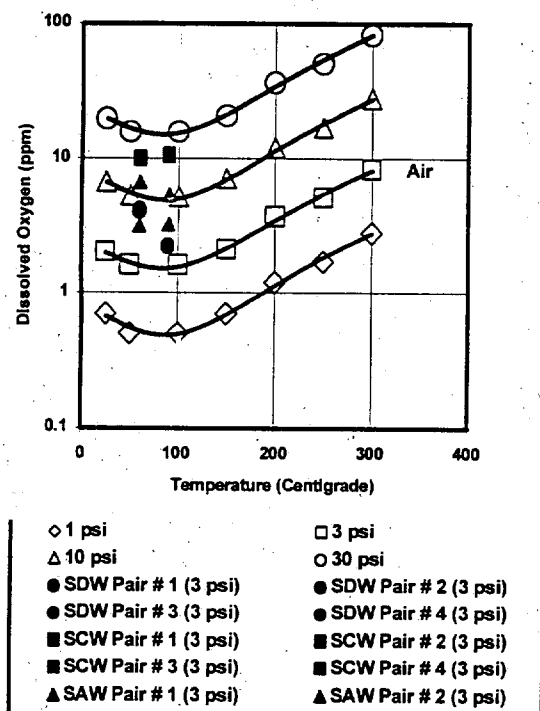


Figure 4. Dissolved Oxygen Measurements in LTCTF to Compared to Published Data for Synthetic Geothermal Brine (Cramer 1974)

Stability of Alloy 22 Passive Film. The localized corrosion model for Alloy 22 assumes that localized attack occurs if the open circuit corrosion potential (E_{corr}) exceeds the threshold (critical) potential for breakdown of the passive film ($E_{critical}$):

$$E_{corr} \geq E_{critical} \quad (\text{Eq. 5})$$

The threshold (critical) potential can be defined in terms of either an initiation potential, or more conservatively, in terms of a repassivation potential. The repassivation potential is the level at which a failed passive film

repassivates, or heals, thereby protecting the surface. Compared to materials proposed for use in earlier WP designs, Alloy 22 has superior resistance to localized corrosion.

Cyclic Polarization Measurements. The YMP has used cyclic polarization (CP) to determine threshold potentials for Alloy 22 in test media relevant to the environment expected in the repository. CP measurements have been based on a procedure similar to ASTM G 5-87 (ASTM 1989), with slight modification. For example, ASTM G 5-87 calls for an electrolyte of 1N H_2SO_4 , whereas SDW, SCW, SAW, SSW and BSW are used here. Furthermore, aerated solutions were used here, unlike the procedure that calls for de-aerated solutions. It has been found that the CP curves for Alloy 22 and stainless steel 316L can be categorized as Type 1, 2 or 3.

Type 1 Polarization Curves. A generic Type 1 curve exhibits complete passivity (no passive film breakdown) between the corrosion potential and the point defined as Threshold Potential 1. This threshold is in the range where the onset of oxygen evolution is expected and is defined by a large excursion in anodic current. This particular definition of Threshold Potential 1 is specific to Type 1 curves. Type 1 behavior has only been observed with Alloy 22 and is illustrated by Figure 5. The interpretation of Type 1 curves as exhibiting no passive film breakdown is consistent with Section 7 of ASTM G61-86 (ASTM 1997c). Furthermore, this interpretation has been verified by visual inspection of samples after potential scans, with photographic documentation of some of those samples (all samples are held in the archives at LLNL).

Type 2 Polarization Curves. A generic Type 2 curve exhibits a well-defined oxidation peak at the point defined as Threshold Potential 1. Threshold Potential 2 is in the range where the onset of oxygen evolution is expected and is defined by a large increase in anodic current. These particular definitions of threshold potentials are specific to Type 2. Repassivation Potentials 1 and 2 are defined as the points where the hysteresis loop passes through current levels of 4.27×10^{-6} and 10^{-5} amps, respectively. Repassivation Potential 3 is determined from the first intersection of the hysteresis loop (reverse scan) with the forward scan. Type 2 is observed with both Alloy 22 and 316L. Definitions of the threshold and repassivation potentials are somewhat subjective, and may vary from investigator to investigator. Scully et al. (1999) define the threshold potential for crevice corrosion of Alloy 22 as the point during the scan of electrochemical potential in the forward direction where the current density increases to a level of 10^{-6} to $10^{-5} \text{ A cm}^{-2}$. Gruss et al. (1998) define the repassivation potential as the point where the current density drops to 10^{-6} to $10^{-7} \text{ A cm}^{-2}$, which is comparable to the definition of Repassivation Potential 3.

CP measurements of Pt in SCW at 90°C were made to serve as a basis of comparison for similar measurements with Alloy 22 and other materials of interest. From such comparisons, it is concluded that the anodic oxidation peak observed in Type 2 curves (between 200 and 600 mV) is due to an anodic reaction of the Alloy 22 passive film. No anodic oxidation peak is observed in the measurement of platinum.

SSW is a saturated sodium-potassium-chloride-nitrate electrolyte, formulated to represent the type of concentrated electrolyte that might evolve on a hot WP surface. This formulation has a boiling point of approximately 120°C at ambient pressure. It is evident in Figure 3 that Alloy 22 maintains passivity at potentials up to the reversal potential (1200 mV versus Ag/AgCl), even under these relatively hostile conditions.

In regard to Type 2 polarization curves for Alloy 22 in SCW, the electrochemical process leading to the anodic oxidation peak (leading edge at approximately 200 mV versus Ag/AgCl) cannot be determined from the CP data alone. This peak is probably due to some change in the oxidation state of the passive film and probably has very little to do with any loss of passivity. To augment these potentiodynamic measurements, potentiostatic polarization tests have been performed. Current transients have been measured while polarizing Alloy 22 at 200 mV versus Ag/AgCl in SCW at 90°C, which is close to the potential where the leading edge of the anodic oxidation peak is located. The current initially increases to a maximum of approximately 25 microamps per square centimeter (the sample size is approximately 0.96 cm²) at 9 hours. This corresponds to a typical non-equilibrium passive current density measured for Alloy 22 at this potential in the absence of the anodic oxidation peak. For example, see a Type 1 polarization curve for Alloy 22 in SAW. Therefore, in regard to Type 2 polarization curves, the anodic oxidation peak does not define any localized corrosion or loss in passivity. Furthermore, Threshold Potential 1 (leading edge of the anodic oxidation peak at approximately 200 mV versus Ag/AgCl) should not be used as the basis for switching on localized corrosion of Alloy 22. Here, it is also assumed that Threshold Potential 2 represents the lower bound for breakdown of the passive film.

Type 3 Polarization Curves. A generic Type 3 curve exhibits a complete breakdown of the passive film and active pitting at potentials relatively close to the Corrosion Potential (E_{corr}). In this case, Threshold Potential 1 corresponds to the critical pitting potential. In regard to the three materials involved in the EDA II design, Type 3 behavior has only been observed with 316L.

Overview of CP Measurements. The CP data obtained thus far are for test media believed to be representative of the expected repository environment. In such test media and at plausible electrochemical potentials, it does not appear that there will be significant localized breakdown of the passive film. Furthermore, relatively wide crevices (110 to 540 microns) formed from passive Alloy 22 do not appear to undergo significant increases in hydrogen ion concentration (pH suppression) at reasonable electrochemical potentials. These potentials are generally below the thresholds determined by CP. Finally, Alloy 22 crevices exposed in the LTCTF do not indicate significant crevice corrosion.

It should be noted that the University of Virginia has very recently (since preparation of this AMR) generated some CP data with very tight crevices and concentrated electrolytes consisting of 5 M LiCl, 0.24 to 0.024 M NaNO₃, 0.026 to 0.26 M Na₂SO₄, and HCl (Scully et al. 1999). Testing was conducted at two temperature levels,

80 and 95°C. The crevices were assembled with a circular sample having a hole in the center to accommodate a bolt, a multiple crevice-forming washer, PTFE tape, a bolt to hold the assembly together, and an applied torque of 70 inch pounds. Under these circumstances, some electrochemical activity indicative of crevice corrosion was observed at potentials ranging from 71 to 397 mV versus Ag/AgCl, depending upon the composition of the electrolyte. Using a current density criterion for repassivation of 10⁻⁵ A cm⁻², repassivation potentials were determined to be slightly above, but relatively close to the open-circuit corrosion potential.

While these concentrated lithium-chloride based electrolytes are not believed to be directly relevant to those conditions anticipated in the repository, the University of Virginia data point out that no attitude of complacency should be adopted in regard to conducting further research in the area of localized corrosion of Alloy 22. Unlike compositions based upon J-13 well water, these electrolytes have no buffer ions *per se*. Clearly, additional work is needed to better understand the passivity and resistance to localized attack of all WP materials. In the future, similar measurements with test media believed to be relevant to the repository should be conducted. Specifically, testing with the tight-crevice geometry used by the University of Virginia and standard electrolytes such as SDW, SCW, SAW, and SSW should be conducted. As more data become available, the correlations for the corrosion and threshold potentials should be updated, expressing these quantities in terms of temperature, pH, and the concentrations of various ions. The effect of welding and aging should also be accounted for. This publication should be viewed as works in progress, with each new version reflecting an evolving level of understanding.

Effect of Thermal Aging. The WP temperature must be kept below 350°C to prevent degradation of cladding on spent nuclear fuel. It is now believed that the WP surface temperature will remain below 300°C. With these constraints, the impact of thermal aging and phase instability on the corrosion of Alloy 22 are expected to be minimal. An extrapolation of the curves given in the companion AMR on aging and phase stability by Summers (2000) does not indicate that the phase stability of Alloy 22 base metal will be a problem at less than about 300°C. However, it must be emphasized that such estimates are preliminary and uncertain. Much additional work is needed in this area. Rebak et al. (1999) have investigated the effects of high-temperature aging on the corrosion resistance of Alloy 22 in concentrated hydrochloric acid. However, due to the temperature used to age the samples (922-1033 K) and the extreme test media used (boiling 2.5% HCl and 1 M HCl at 339 K), these data are not considered relevant to performance assessment for the repository.

Samples of Alloy 22 were aged at 700°C for either 10 or 173 hours. The corrosion resistance of these aged samples is compared to that of base metal in various standardized test media. The Figure 5 shows a comparison of CP curves for base metal and thermally aged material in SAW at 90°C. Both curves exhibit generic Type 1 behavior. In this case, aging appears to shift the corrosion potential to less noble values from -176 to -239 mV versus

a standard Ag/AgCl reference electrode. The passive current density may be increased slightly, which would be indicative of a slight increase in corrosion rate. The highest non-equilibrium passive current observed for the base metal is approximately $4 \mu\text{A cm}^{-2}$ compared to approximately $10 \mu\text{A cm}^{-2}$ for fully aged material. CP curves for base metal and thermally aged material in SCW at 90°C show the anodic oxidation peak that is characteristic of generic Type 2 behavior. In these cases, aging shifts the corrosion potential to less noble values, from -237 to between -328 and -346 mV versus a standard Ag/AgCl reference electrode.

In the tests with BSW-13 shown in Figure 5, aging also appears to shift the corrosion potential to less noble values. A sample aged for only 10 hours has a corrosion potential of only -227 mV versus a standard Ag/AgCl reference electrode, whereas a sample aged for 173 hours has a corrosion potential of -372 mV relative to the same reference. The difference $E_{\text{critical}} - E_{\text{corr}}$ is about 800 mV for an aged sample in either SAW and BSW. The non-equilibrium current densities (corrosion rates) at 0 mV are also similar. However, more quantitative test are required for any definitive statements regarding corrosion rate.

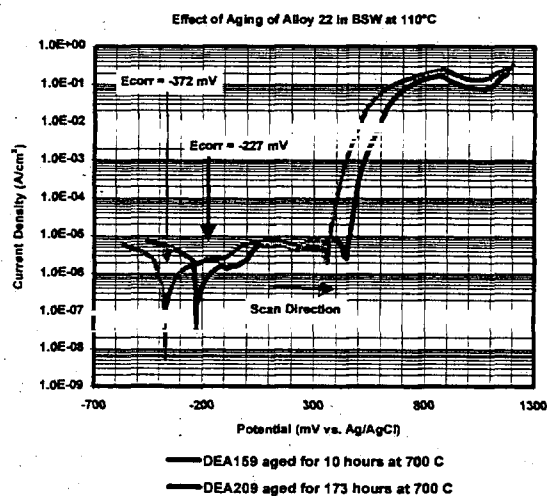


Figure 5. Effect of thermal aging at 700°C on the corrosion resistance of Alloy 22 in BSW-13 at 110°C .

Effect of Gamma Radiolysis. Anodic shifts in the open circuit corrosion potential of stainless steel have been experimentally observed (Glass et al. 1986; Kim 1987, 1988, 1999a, 1999b). It is believed that this observation is due to the generation of hydrogen peroxide. Glass et al. performed ambient-temperature CP of 316L samples in 0.018 M NaCl solution during exposure to 3.5 Mrad h^{-1} gamma radiation (1986). They found that the corrosion current shifted in the anodic direction by approximately 200 mV. From inspection of the graphical data in this article, it is concluded that there is very little increase in the corresponding corrosion current density. However, the separation between the corrosion potential and the threshold for localized attack decreased slightly. This shift in corrosion potential was shown to be due to the formation of hydrogen peroxide. This finding was subsequently confirmed by Kim (1988). In this case, ambient-

temperature CP of 316 stainless steel in acidic ($\text{pH} \sim 2$) 1.5 M NaCl during exposure to 0.15 Mrad h^{-1} gamma radiation showed a 100 mV anodic shift in the corrosion potential, with very little effect on the corrosion current. Note that Glass et al. (1986) and Kim (1988) worked on stainless steels, not Alloy 22.

Additional studies of the corrosion and threshold potentials of Alloy 22 in the presence of gamma radiation, as done by Glass et al. in the early 1980's, is beyond the YMP's current work scope. To determine the maximum impact that gamma radiolysis could have on the corrosion potential, hydrogen peroxide was added to electrolytes used for testing Alloy 22. As the concentration of hydrogen peroxide in SAW approaches 72 ppm (calculated from number of added drops of H_2O_2), the corrosion potential asymptotically approaches 150 mV versus Ag/AgCl, well below any threshold where localized attack would be expected in SAW. Similarly, as the concentration of hydrogen peroxide in SCW approaches 72 ppm, the corrosion potential asymptotically approaches -25 mV versus Ag/AgCl, well below any threshold where localized attack would be expected in SCW. This change in corrosion potential is also below any level where a change in oxidation state would be expected. Since extremely high radiation levels would be required to achieve such shifts in corrosion potential and since even the maximum shifts in potential would be less than those required for breakdown of the passive film, it seems unlikely that gamma radiolysis will lead to catastrophic failure of Alloy 22 due to LC. However, as more resources become available, actual tests with a gamma source should be performed.

General Corrosion Rates. The Long Term Corrosion Test Facility (LTCTF) provides a very good source of corrosion data for Alloy 22 in environments relevant to the proposed high-level waste repository at Yucca Mountain. The LTCTF and results from that facility are described in detail in previous publications by the YMP (Estill 1998). The GC rates of Alloy 22 measured in the LTCTF should be representative of those expected in the repository. Testing includes a wide range of plausible generic test media, including SDW, SCW, SAW, and Simulated Cement-Modified Water (SCMW). The SCW test medium is three orders-of-magnitude ($1000\times$) more concentrated than J-13 well water and is slightly alkaline ($\text{pH} \sim 8$). The SAW test medium is three orders-of-magnitude ($1000\times$) more concentrated than J-13 well water and is acidic ($\text{pH} \sim 2.7$) to mimic the evaporative concentration of electrolytes on the hot WP surface. Concentrated solutions are intended to mimic the evaporative concentration of the electrolytes on the hot WP surface. Two temperature levels (60 and 90°C) are included. The maximum observed rate, which is much less than $1 \mu\text{m per year}$, clearly indicates that the life of the Alloy 22 outer barrier will not be limited by GC. It is also assumed that the corrosion rate is constant, and does not decay with time. Less conservative corrosion models assume that the rate decays with time.

This facility is equipped with an array of fiberglass tanks. Each tank has a total volume of $\sim 2000 \text{ L}$ and is filled with $\sim 1000 \text{ L}$ of aqueous test solution. The solution in a particular tank is controlled at either 60 or 90°C , covered with a blanket of air flowing at approximately $150 \text{ cm}^3 \text{ min}^{-1}$, and agitated. The descriptions and compositions

of three of these solutions are summarized in Table 3. Four generic types of samples, U-bends, crevices, weight loss samples, and galvanic couples, are mounted on insulating racks and placed in the tanks. Approximately half of the samples are submersed, half are in the saturated vapor above the aqueous phase, and a limited number are at the water line. It is important to note that condensed water is present on specimens located in the saturated vapor.

After racks of samples were removed from the tank, samples were first rinsed with deionized water to remove salt solutions. Samples discussed have generic weight-loss or crevice geometry. Generic weight-loss samples were rectangular in shape (1 inch wide, 2 inches long, 1/8 inch thick). Generic crevice samples were square with a hole in the center (2 inches on each side, 1/8 inch thick, with a 0.312 inch diameter hole). Next, samples were removed from the rack by loosening fixture mounts with standard wrenches. The crevice assemblies described by Estill (1998) required further disassembly, which was also done with standard wrenches. After dismounting and disassembly, the metal samples of Alloy 22 were cleaned with the solution designated C.7.5 for stainless steels given in Table A1 of ASTM G 1-90 (ASTM 1997e). This solution consists of 100 ml HNO₃ (specific gravity ~ 1.42) and 20 ml HF (specific gravity ~ 1.198) in enough water to give a total volume of 1000 ml. Note that alternative solutions for nickel and nickel-based alloys, designated C.6.1 and C.6.2, could have also been used. These cleaner formulations are based upon aqueous solutions of HCl and H₂SO₄, respectively.

The crevice samples were configured in such a way as to reveal crevice corrosion if it occurred. Since no crevice attack was observed with the samples represented by these figures, it is assumed that all weight loss in the crevice samples was due to GC outside of the crevice region (area underneath washer). This is consistent with other *ex situ* examinations.

As previously discussed, GC measurements are based upon ASTM G 1-81 (ASTM 1987), or the more recent ASTM G 1-90 (ASTM 1997e). The GC (or penetration) rate of an alloy can be calculated from weight loss data as follows with the following general formula. This formula for corrosion rate can be rewritten in the following form:

$$\frac{dp}{dt} = \frac{w}{\rho \times t [2(a \times b) + 2(b \times c) + 2(a \times c)]} \quad (\text{Eq. 6})$$

where dp/dt is the corrosion (penetration) rate, w is the mass loss in grams, ρ is the density in grams per cubic centimeter, t is the time of exposure in years, and the quantity in square brackets represents the exposed area of the sample in square centimeters. Without application of any conversion factor, the corrosion rate calculated with this formula has the units of centimeters per year. Multiplication of dp/dt by $10^4 \mu\text{m cm}^{-1}$ yields a corrosion rate with the units of μm per year. The weight loss and dimensional change were measured with electronic instruments calibrated to traceable standards. All data was digitally transferred to computer, minimizing the possibility of human typographical error.

GC rates for Alloy 22 based on LTCTF weight loss samples exposed for six and twelve months are shown in

Figure 6. It appears that these measurements are independent of temperature between 60 and 90°C. Furthermore, the composition of the test medium (SDW, SCW or SAW) appeared to have little impact on the measurements. Since the maximum observed rate is only 160 nm y^{-1} , it is concluded that the actual corrosion rate is below the detectable level. When all of the measured corrosion rates based upon the weight loss samples are ranked together, regardless of the test medium or temperature, the data appear to be normally distributed around a median value.

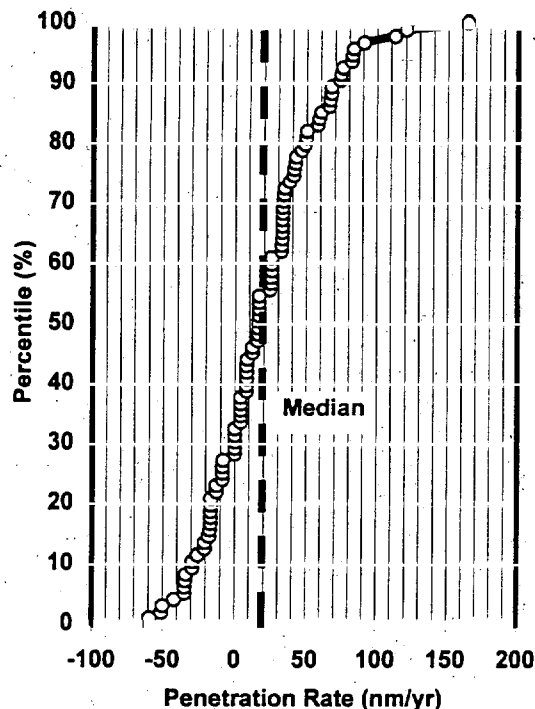


Figure 6. Distribution of General Corrosion Rates for Alloy 22 – LTCTF Measurements

The GC rates for Alloy 22 based on LTCTF crevice samples also appear to be independent of temperature and test medium. When all of the measured corrosion rates based upon the weight loss samples are ranked together, most of the data points fall below 160 nm y^{-1} and appear to be normally distributed around a median value. However, there are four data points that appear to lie above the detection limit (between 200 and 750 nm , per year). Since no crevice attack of these four samples is evident with microscopic examination, it is believed that these points are due to the accidental removal of material during mechanical assembly of the crevice sample. The largest measured rate will not lead to failure of the WP during the 10,000 year service life. Based upon these data, it does not appear that the life of the WP will be limited to less than 10,000 years by the GC of Alloy 22 at temperatures less than those involved in the test (90°C).

The mean and standard deviation are also determined through calculation (Burr 1974). The average corrosion rate based upon all weight loss samples is 20 nm y^{-1} , with a standard deviation of 40 nm y^{-1} . The average corrosion rate

based upon all crevice samples is 71 nm y⁻¹, with a standard deviation of 89 nm y⁻¹. If the four highest rates are omitted, the average rate is then calculated to be 57 nm y⁻¹, with a standard deviation of 40 nm y⁻¹.

It should be noted that the distribution of corrosion rates includes some negative values. The negative corrosion rates correspond to cases where the samples actually appear to have gained weight during exposure, due to oxide growth or the formation of silicate deposits. To substantiate these interpretations, AFM has been used to inspect a number of samples removed from the LTCTF.

Formal Error Analysis. The general method used in the formal error analysis is now presented and is important since it enables sound interpretation of the data shown in Figure 6. Consider the dependent variable y defined by the following generic function:

$$y = f(x_1, x_2, x_3, x_4 \dots x_n) \quad (\text{Eq. 7})$$

where x_i is the i^{th} independent variable. The total derivative of y is then defined as follows:

$$dy = \frac{\partial y}{\partial x_1} dx_1 + \frac{\partial y}{\partial x_2} dx_2 + \frac{\partial y}{\partial x_3} dx_3 + \frac{\partial y}{\partial x_4} dx_4 + \dots + \frac{\partial y}{\partial x_n} dx_n \quad (\text{Eq. 8})$$

Based upon this definition, the maximum error in y can then be defined as:

$$\Delta y = \left| \frac{\partial y}{\partial x_1} \Delta x_1 \right| + \left| \frac{\partial y}{\partial x_2} \Delta x_2 \right| + \left| \frac{\partial y}{\partial x_3} \Delta x_3 \right| + \left| \frac{\partial y}{\partial x_4} \Delta x_4 \right| + \dots + \left| \frac{\partial y}{\partial x_n} \Delta x_n \right| \quad (\text{Eq. 9})$$

where Δx_i is the error in the i^{th} independent variable. Let the dependent variable y be the GC rate measured in the LTCTF.

$$y = \frac{dp}{dt} = \frac{w}{\rho \times t} \frac{1}{[2(a \times b) + 2(b \times c) + 2(a \times c)]} \quad (\text{Eq. 10})$$

The total derivative of the corrosion rate is

$$dy = \frac{\partial y}{\partial w} dw + \frac{\partial y}{\partial \rho} d\rho + \frac{\partial y}{\partial t} dt + \frac{\partial y}{\partial a} da + \frac{\partial y}{\partial b} db + \frac{\partial y}{\partial c} dc \quad (\text{Eq. 11})$$

The maximum error in the corrosion rate is

$$\Delta y = \left| \frac{\partial y}{\partial w} \Delta w \right| + \left| \frac{\partial y}{\partial \rho} \Delta \rho \right| + \left| \frac{\partial y}{\partial t} \Delta t \right| + \left| \frac{\partial y}{\partial a} \Delta a \right| + \left| \frac{\partial y}{\partial b} \Delta b \right| + \left| \frac{\partial y}{\partial c} \Delta c \right| \quad (\text{Eq. 12})$$

The partial derivatives are:

$$\frac{\partial y}{\partial w} = \frac{1}{\rho \times t} \frac{1}{[2(a \times b) + 2(b \times c) + 2(a \times c)]} \quad (\text{Eq. 13})$$

$$\frac{\partial y}{\partial \rho} = \frac{w}{\rho^2 \times t} \frac{1}{[2(a \times b) + 2(b \times c) + 2(a \times c)]} \quad (\text{Eq. 14})$$

$$\frac{\partial y}{\partial t} = \frac{w}{\rho \times t^2} \frac{1}{[2(a \times b) + 2(b \times c) + 2(a \times c)]} \quad (\text{Eq. 15})$$

$$\frac{\partial y}{\partial a} = \frac{w}{\rho \times t} \frac{[2b + 2c]}{[2(a \times b) + 2(b \times c) + 2(a \times c)]^2} \quad (\text{Eq. 16})$$

$$\frac{\partial y}{\partial b} = \frac{w}{\rho \times t} \frac{[2a + 2c]}{[2(a \times b) + 2(b \times c) + 2(a \times c)]^2} \quad (\text{Eq. 17})$$

$$\frac{\partial y}{\partial c} = \frac{w}{\rho \times t} \frac{[2a + 2b]}{[2(a \times b) + 2(b \times c) + 2(a \times c)]^2} \quad (\text{Eq. 18})$$

The maximum error in the corrosion rate is estimated by calculating numeric values of the partial derivatives from expected values of the independent variables, multiplication of each partial derivative by the corresponding error in independent variable (Δw , $\Delta \rho$, Δt , Δa , Δb , and Δc), and summation of the resulting products. The error based upon this method is shown in Table 5.

From the estimated errors given in Table 5, it is concluded that the typical uncertainty observed in weight loss and dimensional measurements prevent determination of corrosion rates less than approximately 38 nm y⁻¹. The maximum uncertainty is estimated to be approximately 6 to 20 nm y⁻¹ in the case of crevice samples and 11 to 38 nm in the case of weight loss samples. These estimates of probable error are believed to correspond to about one standard deviation (1 σ). Therefore, any measured corrosion rate greater than 160 nm y⁻¹ (4 σ) should be easily distinguishable from measurement error. Any rate less than 160 nm y⁻¹ guarantees that the WP outer barrier (wall thickness of 2 cm) will not fail by GC.

Table 5. Summary of Error Analysis for Corrosion Rates Based Upon Weight Loss Measurements

	Assumed Weight Loss		0.0001 g	0.0010 g	0.0100 g
			Δy	Δy	Δy
Case	Sample Configuration	Exposure Time	nm y^{-1}	nm y^{-1}	nm y^{-1}
1	Crevice	6 month	12.25	12.95	19.86
2	Weight Loss	6 month	23.27	24.64	38.33
3	Crevice	12 month	6.00	6.29	9.17
4	Weight Loss	12 month	11.40	11.98	17.72

Atomic Force Microscopy. The AFM has been used to characterize the surface topographies of weight-loss coupons of Alloy 22 that had been exposed to various environments in the YMP's LTCTF for one year. Having sub-nm vertical resolution, the AFM is an ideal tool for detecting extremely small penetrations in corrosion-resistant materials such as Alloy 22. Bedrossian and Fix have applied this technique to five Alloy 22 samples used for weight loss measurements (Farmer 2000). These samples include an unexposed control sample and samples exposed to aqueous-phase SAW, vapor-phase SAW, aqueous-phase SCW, and vapor-phase SCW. After the samples were removed from the LTCTF, they were ultrasonically agitated in deionized water, acetone, and methanol for ten minutes each. The Digital Instruments DM3100 AFM was then used for imaging. Each set of data consists of a large-area scan ($25 \mu\text{m} \times 25 \mu\text{m}$), followed by smaller-area details of the region displayed in the large-area scan.

The gross surface topography is dominated by the machining grooves, with typical heights of several hundred nm and typical lateral periodicities of several μm , features plainly visible on images of the control sample (Figure 7). Samples removed from the LTCTF exhibit varying degrees of coverage by a deposit on top of this gross topography. The AFM images show that the most extensive deposit formation occurred on the sample exposed to aqueous-phase SAW (Figure 8). The next most extensive deposit formation occurred on the sample exposed to vapor-phase SAW. X-ray Diffraction scans of all five coupons show that the deposit is predominantly a silicate or SiO_2 , with some NaCl appearing on the two samples which were in the SAW tank. Based upon both AFM and XRD data, the two samples exposed to SCW showed lesser degrees of coverage by the silicate deposit. In some cases, depressions can be seen in the silicate deposit. However, it is not believed that any of these penetrate to the underlying metal.

At the present time, there is insufficient data to quantitatively determine the extent of silicate removal from exposed Alloy 22 samples by acid cleaning. In the future, an effort will be made to collect sufficient quantitative information to quantitatively determine how much silicate remains on the surface after the acid cleaning procedure. In the mean time, a worst-case estimate of the impact of SiO_2 on measured corrosion rates will be used.

The formation of SiO_2 deposits on the surface of the Alloy 22 could bias the distribution of GC rate shown in

Figure 6. From various AFM images of Alloy 22 samples removed from the LTCTF, it appears that a typical deposit can have a thickness as great as 0.25 microns after 12 months of exposure. The resultant bias is then estimated. It is assumed that the deposit has the density of lechatelierite (amorphous SiO_2), which is approximately 2.19 g cm^{-3} (Weast 1978 p. B-161). It is further assumed that the surface is completely and uniformly covered by this deposit. The estimated surface areas of the weight-loss and crevice samples are 30.65 and 57.08 cm^2 , respectively (4.75 and 8.85 in^2 , respectively). Consequently, the deposit thickness translates into a mass change of 1.678 and 3.125 mg for weight-loss and crevice samples, respectively, after 12 months of exposure. Equation 6 is then applied to determine the impact of such a positive mass change on the calculated GC rate. In the case of the weight loss sample, the estimated bias is 0.063 microns per year (63 nm y^{-1}). In the case of the crevice sample, the result is the same. The distribution of GC rate shown in Figure 6 can be corrected for the maximum bias due to SiO_2 deposit formation by adding a constant value of 63 nm y^{-1} to each estimated value of the GC rate. This is equivalent to shifting the curves shown in Figure 6 to the right by sixty-three nanometers per year (63 nm y^{-1}).

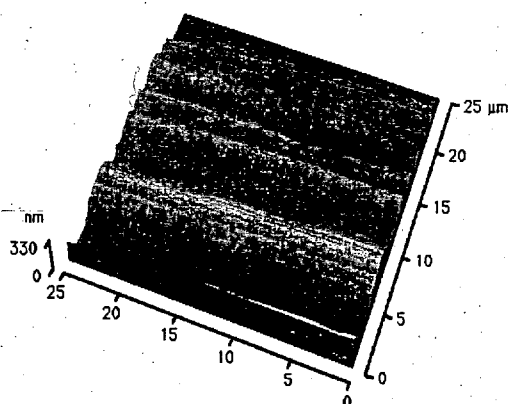


Figure 7. AFM Image of Alloy 22 Control Sample

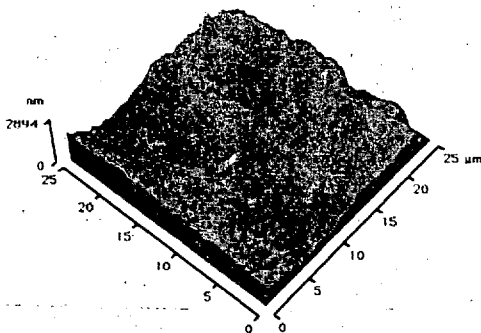


Figure 8. AFM Image of Alloy 22 Sample Removed from LTCTF

Crevice Corrosion. At points of contact between the WP and other solid objects, crevices form occluded geometries, which lead to differential aeration of the crevice solution (electrolyte). Dissolved oxygen can become depleted deep within the crevice, while the oxygen concentration near the crevice mouth remains relatively high. Cathodic reduction of dissolved oxygen at the crevice mouth may create a sufficiently high electrochemical potential to drive anodic processes inside the crevice, thereby causing an anodic current to flow along the crevice towards the crevice mouth. Under realistic repository conditions, it is believed that the walls of the Alloy 22 crevice will remain passive. The potential at the mouth of a crevice is expected to be well below the threshold for localized attack, as determined with CP measurements. Anodic processes inside the crevice are, therefore, expected to occur at a rate that corresponds to the local passive current density. Two primary electrochemical processes can lead to acidification of the solution in a passive crevice, (1) the preferential transport of anions into the crevice from the mouth driven by the electric field that accompanies the crevice current and (2) hydrolysis reactions of dissolved metal cations. Based upon experimental work with passive crevices without buffer, it is believed that the applied potentials required for significant acidification ($\text{pH} < 5$) are not plausible. A minimum crevice pH of approximately 5 is assumed. Additional experimental work of the type discussed here is required to further substantiate this preliminary conclusion.

A detailed deterministic model has been developed to calculate the spatial distributions of electrochemical potential and current density in WP crevices, as well as transient concentration profiles of dissolved metals and ions (Farmer and McCright 1998; Farmer et al. 1998). These quantities are calculated with the transport equations, which govern electromigration, diffusion, and convective transport. In cases with strong supporting electrolyte, electromigration can be ignored (Newman 1991). First, the axial current density along the length of the crevice is

calculated by integrating the wall current density. The electrode potential along the length of the crevice can then be calculated from the axial current density. This technique is similar to that employed in other models (Nystrom et al. 1994). Such models show that the electrochemical potential decreases with increasing distance into the crevice. Therefore, the potential should never be more severe (closer to the threshold for LC) than at the crevice mouth. The partial differential equations that define transient concentrations in the crevice require determination of the potential gradient, as well as the local generation rates for dissolved species. The concentrations of dissolved metals at the crevice mouth are assumed to be zero. Computations are facilitated by assuming that the crevices are symmetric about a mirror plane where the flux is zero. This model has been used to estimate the extent of pH suppression in WP crevices due to the simultaneous hydrolysis and transport of dissolved alloying elements, which include Fe, Ni, Cr, Mo and W.

The local crevice environments for Alloy 22 and other relevant materials are being determined experimentally. Crevices have been constructed from square metallic samples, 2 inches on each side and 1/8 inch thick (same size as crevice samples used in the LTCTF). The samples are masked with plastic tape, thereby forming an exposed square area, 1.7 inches on each side. The exposed area is placed underneath a clear plastic window with an access port for a pH sensor in the center. In this case, the sensor is a miniature reference electrode separated from the crevice solution with a thin glass membrane. A second pH sensor is located at the mouth of the crevice, in close proximity to a saturated calomel reference electrode (SCE). The use of in situ sensors to determine crevice pH has also been described by Sridhar and Dunn (1994). In parallel experiments by Farmer et al. (1998), paper strips with a pH-sensitive dye (pH paper) have been sandwiched between the clear plastic window and photographed with a digital electronic camera in a time-lapse mode to add confidence to the measurements made with pH sensors. Spectroscopic-grade graphite counter electrodes are also placed in the electrolyte lying outside the mouth of the crevice. A potentiostat is then used to control the electrochemical potential at the mouth of the crevice. Temperature, potential, current, and pH is then recorded electronically during the course of the experiment.

Measurements of pH inside a crevice formed from 316L stainless steel were made with 4M NaCl at ambient temperature. Since this electrolyte contains no buffer ions, it is considered to be a far more severe medium than those representative of various concentrations of J-13 well water. The electrochemical potential at the mouth was maintained at 200 mV versus Ag/AgCl. Crevice corrosion could be seen initiating near the crevice mouth and propagating towards the pH sensor, which was located about 0.5 cm inside the crevice mouth. When the corrosion front reached the pH sensor, the pH dropped from the initial value ($\text{pH} \sim 7$) to a very low value ($\text{pH} \sim 1$). The fixed one-liter volume of electrolyte outside of the crevice became slightly alkaline. The pH of this solution reached a maximum ($\text{pH} \sim 10$) and then fell to a slightly lower steady-state value ($\text{pH} \sim 9$). Active corrosion inside the crevice is evident since the color of the crevice solution becomes emerald

green. In similar experiments with 316L exposed to SCW, no significant lowering of the pH was observed.

Measurements of pH inside crevices formed with Alloy 22 surfaces were also made. The pH in a crevice with a potential of 800 mV versus Ag/AgCl applied at the mouth was monitored. The electrolyte was 4M NaCl and was maintained at ambient temperature. The Alloy 22 surface remained passive underneath the window, with no visible signs of localized attack. However, the passive current flow from within the crevice was sufficient to cause the pH to be immediately lowered from the initial value (pH~6.5) to a minimum value (pH~3.3), after which the pH gradually increased over several hours (pH~4.5). The fixed one-liter volume of electrolyte outside of the crevice became slightly alkaline (pH~8.3) before the data acquisition was started and dropped gradually over several hours (pH~7). The lowering of pH inside of passive Alloy 22 crevices with high-applied potential has been verified by independent technique-development tests with indicator paper. The applied potential was increased above the threshold required for localized breakdown of the passive film. An applied potential of 1100 mV can drive the pH to extremely low levels (pH~0.2) in Alloy 22 crevices. At an applied potential of 400 mV, the steady-state crevice pH remained close to neutrality (pH~6.1). As the potential was stepped to 1000 mV, which is slightly above the repassivation potential measured by Gruss et al. (1998), the

crevice current increased dramatically and the pH dropped below one. At an applied potential of 1100 mV, extreme localized attack of the Alloy 22 was observed at the crevice mouth, with a crevice pH slightly less than zero. At the end of the experiment, the crevice sensor was immediately submersed in a buffer solution (pH 7) and shown to be in good calibration (virtually no drift during test). The effect of buffer ions on crevice chemistry was investigated. In these studies, SCW was used as the electrolyte. Even at an applied potential of 800 mV, no significant lowering of the pH was observed. The Alloy 22 inside the crevice appeared to be unchanged from its initial state, with no evidence of localized attack.

Figure 9 is a summary of several experiments where crevice pH was determined in situ as a function of applied potential. These data are represented by the following polynomial:

$$y = b_0 + b_1x + b_2x^2 \quad (\text{Eq. 19})$$

where x is the potential applied at the crevice mouth (mV versus Ag/AgCl) and y is the steady-state pH inside the crevice. Coefficients for the above equation are summarized in Table 6 and Figure 9, representing both Alloy 22 and 316L in under a broad range of conditions. The correlations for 4M NaCl and SCW should be used to bound the crevice pH, using linear interpolation between the two limits, based upon the concentration of buffer ion.

Table 6. Coefficients for the Correlation of Crevice pH with Applied Potential

Material	Medium	Crevice Spacer (μm)	b_0	b_1	b_2	R^2
Alloy 22	4M NaCl	110	7.2716	-0.0012	-5.0E-06	0.9782
Alloy 22	4M NaCl	540	7.0227	-0.0015	-4.0E-06	~1
Alloy 22	SCW	540	8.276	0.0003		0.9646
316L	4M NaCl	540	1.035	-0.00001		0.0005
316L	SCW	540	8.1175	-0.00006		~1

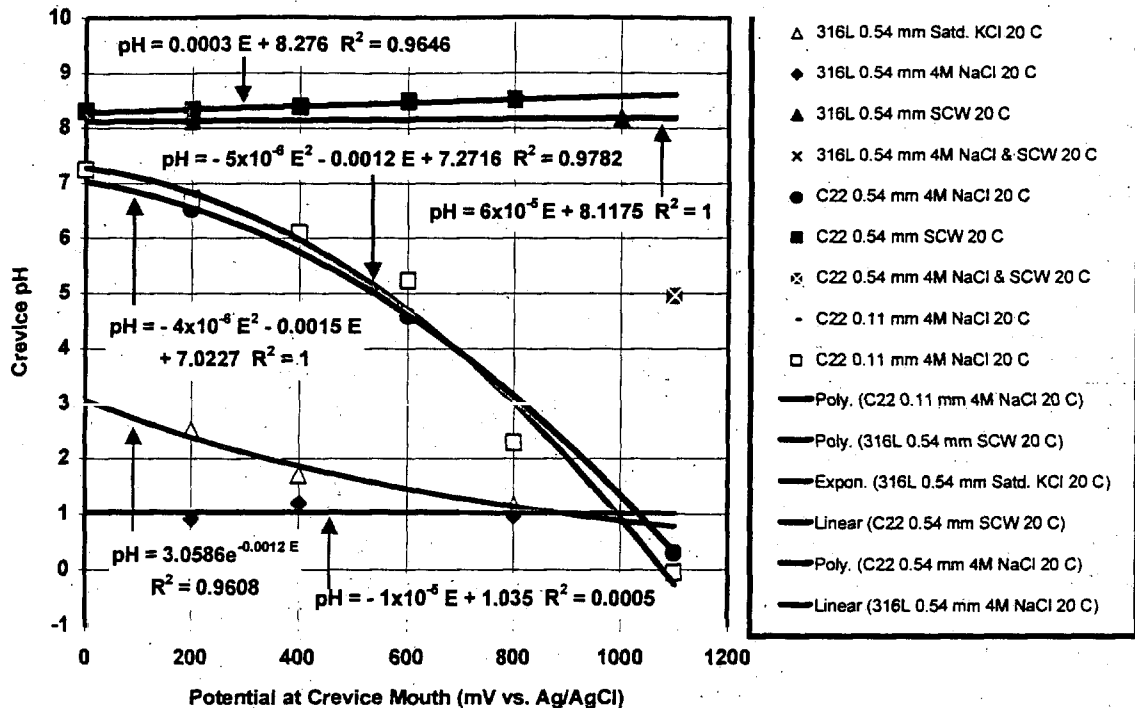


Figure 9. Determination of Crevice pH for WP Materials

In summary, there was no visible evidence of localized corrosion of the metal inside the crevice at applied potentials less than the threshold. However, even though the crevice remained passive, the passive current density and imposed electric field within the crevice was sufficient to cause significant acidification. In many of the experiments described here, both the applied potential and the test medium are more severe than those expected in the repository. However, the temperature of aqueous solutions on the WP surface may be significantly higher (120°C). Work is in progress to obtain comparable data at higher temperature. The experimental data support published numerical simulations (Farmer et al. 1998; Farmer, McCright, Estill and Gordon 1999).

Estimated Rate of Localized Corrosion. If the threshold potential for localized attack is exceeded, a corrosion rate representative of LC must be assumed. Due to the outstanding corrosion resistance of Alloy 22, very little data exists for such localized corrosion under plausible conditions. Work originally published by Asphahani (1980) and later reviewed by Gdowski (1991) indicates that the corrosion rate of Alloy 22 in 10 wt% FeCl₃ at 75°C might be as high as 12.7 μm per year. This rate is significantly higher than those measured in the LTCTF and may be representative of the types of rates expected for LC, including crevice corrosion. In a solution composed of 7 vol. % H₂SO₄, 3 vol. % HCl, 1 wt% FeCl₃, and 1 wt% CuCl₂, a penetration rate of 610 μm per year was observed at 102°C. From other published sources (Sedriks 1996), the corrosion rate of Alloy C-276 in dilute

HCl at the boiling point is somewhere between 5 and 50 mils per year (127 and 1270 μm per year). Comparable rates would be expected for Alloy 22. The highest passive current density observed during CP measurements is approximately 10 μA cm⁻², which corresponds to a corrosion rate of about 100 microns per year. For the time being, it is assumed that the logarithm of the localized corrosion rate of Alloy 22 is normally distributed, with the cumulative distribution function being defined by Table 7. This distribution reasonably bounds those extreme penetration rates found in the literature and is centered around the rate corresponding to the passive current density.

Table 7. Distribution of LC Rates for Alloy 22 (Asphahani 1980, Gdowski 1991; Sedriks 1996)

Percentile (%)	Localized Corrosion Rate (μm per year)
0 th	12.7
50 th	127
100 th	1270

Effect of Thermal Aging. A fully aged sample of Alloy 22 appears to exhibit a less noble corrosion potential, shifted in the cathodic direction by approximately: 63 mV in the case of SAW at 90°C; 109 mV in the case of SCW at 90°C; and by more than 100 mV in the case of BSW at

110°C. It is assumed that E_{corr} can be corrected to account for fully aged material by subtracting approximately 100 mV from values calculated for the base metal. The shift in $E_{critical}$ (Threshold Potential 1) also appears to be approximately 100 mV in most cases. Thus, the difference $E_{critical} - E_{corr}$ appears to be virtually unchanged.

The effect of thermal aging on the corrosion rate is accounted for in the enhancement factor, G_{aged} , and is based upon a ratio of the non-equilibrium current densities for base metal and aged material.

$$\left. \frac{dp}{dt} \right|_{effective} = G_{aged} \times \left. \frac{dp}{dt} \right|_{effective} \quad (\text{Eq. 20})$$

The value of G_{aged} for base metal is approximately one ($G_{aged} \sim 1$), whereas the value of G_{aged} for fully aged material is larger ($G_{aged} \sim 2.5$). Material with less precipitation than the fully aged material would have an intermediate value of G_{aged} ($1 \leq G_{aged} \leq 2.5$).

Effect of Microbial Growth. It has been observed that nickel-based alloys such as Alloy 22 are relatively resistant to microbial influenced corrosion (MIC) (Lian et al. 1999). Furthermore, it is believed that microbial growth in the repository will be limited by the availability of nutrients. For example, H^+ is known to be generated by bacterial isolates from Yucca Mountain. Furthermore, thiobacillus ferro-oxidans oxidize Fe^{2+} , while geobacter metallireducens reduce Fe^{3+} . Other microbes can reduce SO_4^{2-} and produce S^2- . Ultimately, the impact of MIC will be accounted for by adjusting E_{corr} , $E_{critical}$, pH, and the sulfide concentration. The possible acceleration of abiotic corrosion processes by microbial growth is addressed here. Horn (1998-99) has shown that MIC can enhance corrosion rates of Alloy 22 by a factor of at least two (2x). Measurements for Alloy 22 and other similar materials are shown in Table 8. The augmentation of corrosion rates due to MIC are accounted for in the model through the enhancement factor, G_{MIC} .

$$\left. \frac{dp}{dt} \right|_{effective} = G_{MIC} \times \left. \frac{dp}{dt} \right|_{effective} \quad (\text{Eq. 21})$$

This factor is calculated as the ratio of corrosion rates (microbes to sterile) and from Table 8. The value of G_{MIC} for Alloy 22 in sterile media is approximately one ($G_{MIC} \sim 1$), whereas the value of G_{MIC} for Alloy 22 in inoculated media is larger ($G_{MIC} \sim 2$). Assume that G_{MIC} is uniformly distributed between these limits, and that this distribution is half uncertainty and half variability. A patch experiencing both thermal aging and MIC would have a corrosion rate enhanced by the factor $G_{aged} \times G_{MIC}$.

The principal nutrient-limiting factor to microbial growth *in situ* at Yucca Mountain has been determined to be low levels of phosphate. There is virtually no phosphate contained in J-13 groundwater. Yucca Mountain bacteria grown in the presence of Yucca Mountain tuff are apparently able to solubilize phosphate contained in the tuff to support growth to levels of 10^6 cells ml^{-1} of groundwater. When exogenous phosphate is added (10 mM), the levels of bacterial growth increase to 10^7 to 10^8 cells ml^{-1} . The one to two orders-of-magnitude difference in bacterial growth

with and without the presence of exogenous phosphate is almost certainly not significant with respect to effects on corrosion rates. Therefore, nutrient limitation, at least at a first approximation, was not factored into the overall MIC model. It may be noted, however, that the two-fold G_{MIC} included in the model was in the presence of sufficient phosphate to sustain higher levels of bacterial growth (in an effort to achieve accelerated conditions).

Other environmental factors that could effect levels of bacterial growth include temperature and radiation. These factors, however, are closely coupled to RH; as temperature and radiation decrease in the repository, RH is predicted to increase. At the same time, while there are some types of microorganisms that can survive elevated temperatures ($\leq 120^\circ\text{C}$) and high radiation doses if there is no available water, then bacterial activity is completely prevented. Thus, because water availability is the primary limiting factor, and this factor is coupled to other less critical limiting factors, water availability (as expressed by RH) is used as the primary gauge of microbial activity.

Determination of a critical mass of total bacteria required to cause MIC is not an issue that needs to be addressed in the MIC model. Bacterial densities in Yucca Mountain rock have been determined to be on the order of 10^4 to 10^5 cells gm^{-1} of rock. In absolute terms, this is almost certainly above the threshold required to cause MIC. Further, bacterial densities were shown to increase one to two orders-of-magnitude when water is available (above). A more germane concern is the types of bacteria present, their abundance, and how their relative numbers are affected when water is available for growth. Corrosion rates will be affected (at least on some WP materials) for example, if organic acid producers out compete sulfate reducers or inorganic acid producers for available nutrients when water is sufficient to support growth. No data is currently available regarding the composition of the bacterial community over the changing environmental conditions anticipated during repository evolution. Instead, this issue has been addressed in the current model by determining overall corrosion rates under a standardized set of conditions, in the presence and absence of a defined set of characterized Yucca Mountain bacteria. Clearly, more data is required to better predict MIC on any given material with respect to this concern. Corrosion rates are currently being determined in the presence of Yucca Mountain rock containing the complete complement of Yucca Mountain bacteria and under conditions more representative of the repository.

MIC is defined as a localized effect; thus, not all areas are equivalent on any given waste package with respect to bacterial colonization. It is well documented that bacteria preferentially colonize weldments, heat-affected zones, and charged regions (Borenstein and White 1989; Walsh 1989; Enos and Taylor 1996). However, the current model is based on data collected using unwelded specimens. In order to account for preferential areas of colonization in the model, it might be assumed that G_{MIC} is uniformly distributed with respect to areal distribution.

American Society of Mechanical Engineers
Seattle, Washington – July 2000

Table 8. Alterations in Corrosion Potentials Associated with Microbial Degradation (Horn 1999)

Tested Sample Initial Condition	Average Corrosion Rate ($\mu\text{m}/\text{yr}$)	Corrosion Potential E_{corr} (V vs SCE)	
		Initial	Endpoint
CS1020 + YM Microbes	8.8	-0.660	-0.685
Sterile CS 1020	1.4	-0.500	-0.550
M400 + YM Microbes	1.02	-0.415	-0.315
Sterile M400	0.005	-0.135	-0.070
C-22 + YM Microbes	0.022	-0.440	-0.252
Sterile C-22	0.011	-0.260	-0.200
I625 + YM Microbes	0.013	-0.440	-0.285
Sterile I625	0.003	-0.160	-0.130
304SS + YM Microbes	0.035	-0.540	-0.280
Sterile 304SS	0.003	-0.145	-0.065

CONCLUSIONS

Alloy 22 is an extremely corrosion resistant material, with a very stable passive film. Based upon exposures in the LTCTF, the GC rates of Alloy 22 are typically below the level of detection, with four outliers having reported rates up to 0.75 μm per year. In any event, over the 10,000 year life of the repository, GC of the Alloy 22 (assumed to be 2 cm thick) should not be life limiting. Because measured corrosion potentials are far below threshold potentials, localized breakdown of the passive film is unlikely under plausible conditions, even in SSW at 120°C. The pH in ambient-temperature crevices formed from Alloy 22 have been determined experimentally, with only modest lowering of the crevice pH observed under plausible conditions. Extreme lowering of the crevice pH was only observed under situations where the applied potential at the crevice mouth was sufficient to result in catastrophic breakdown of the passive film above the threshold potential in non-buffered conditions not characteristic of the Yucca Mountain environment. In cases where naturally occurring buffers are present in the crevice solution, little or no lowering of the pH was observed, even with significant applied potential. With exposures of twelve months, no evidence of crevice corrosion has been observed in SDW, SCW, and SAW at temperatures up to 90°C. An abstracted model has been presented, with parameters determined experimentally, that should enable performance assessment to account for the general and localized corrosion of this material. A feature of this model is the use of the materials specification to limit the range of corrosion and threshold potentials, thereby making sure that substandard materials prone to localized attack are avoided. Model validation will require future confirmatory testing.

ACKNOWLEDGEMENTS

Work was sponsored by the U.S. Department of Energy Office of Civilian and Radioactive Waste Management (OCRWM). This work was done under the

auspices of the U.S. Department of Energy (DOE) by Lawrence Livermore National Laboratory (LLNL) under Contract No. W-7405-Eng-48.

Contributing researchers include Ken King, Steve Gordon, Larry Logotetta, Beverly Lum, David Fix and others. Technical comments by James Blink, Gerry Gordon, Venkataraman Pasupathi, Bob Andrews, Joon Lee, Kevin Mon, and members of the Nuclear Waste Technical Review Board (NWTRB) are gratefully acknowledged. Data qualification was coordinated by Michael Coatsworth and Tom Gibson, with editorial work by Kim Hermann. QA comments by Charlie Warren and Richard Powe are appreciated. Direct management and oversight included George Dials, Dan Wilkens, Jean Younker, Mike Lugo, Hugh Benton, David Stahl, Terry Surles, Martha Kohler and Cynthia Palmer.

REFERENCES

- ASTM 1987. Designation G 1-81, *1987 Annual Book of ASTM Standards*, Section 3, Vol. 3.02, pp. 89-94.
- ASTM 1989. Designation G 5-87, *1989 Annual Book of ASTM Standards*, Section 3, Vol. 3.02, pp. 79-85.
- ASTM 1997a. Designation B 575-94, *1997 Annual Book of ASTM Standards*, Section 2, Vol. 2.04, pp. 409-410, Subsection 7.1.
- ASTM 1997c. Designation G 61-86, *1997 Annual Book of ASTM Standards*, Section 3, Vol. 3.02, pp. 231-235.
- ASTM 1997e. Designation G 1-90, *1997 Annual Book of ASTM Standards*, Section 3, Vol. 3.02, pp. 15-21.
- Asphahani, A.I. 1980. *Materials Performance* 19 12, 33-43.
- Borenstein, S.W. and White, D.C. 1989. Paper 183, *Corrosion 98*, NACE, Houston, TX.
- Burr, I.W. 1974. Chapter 6, *Applied Statistical Methods*, Academic Press, New York, NY, p. 138.

**American Society of Mechanical Engineers
Seattle, Washington – July 2000**

- Cramer, S.D. 1974. *Corrosion Problems in Energy Conversion and Generation*, C.S. Tedman, Jr., Ed., Corrosion Division, ECS, Princeton, NJ, pp. 251–262.
- Civilian Radioactive Waste Management (CRWMS) Management and Operating Contractor (M&O) 1999. License Application Design Selection (LADS) Report, B00000000-01717-4606-00123 Rev. 01 ICN 01, CRWMS M&O, Las Vegas, NV.
- Enos, D.G. and Taylor, S.R. 1996. *Corrosion* 52 11, 831–842.
- Estill, J.C. 1998. *Engineered Materials Characterization Report*, R.D. McCright, Editor, Lawrence Livermore National Laboratory, UCRL-ID-119564, Vol. 3, Rev. 1.1, Section 2.2, pp. 2.2-1 through 2.2-103.
- Evans, M.; Hastings, N.; and Peacock, B. 1993. *Statistical Distributions*, 2nd Edition, John Wiley & Sons, New York, NY, pp. 149–150.
- Farmer, J.C. and McCright, R.D. 1998. Paper No. 160, *Corrosion* 98, NACE, Houston, TX.
- Farmer, J.C., et al. 1998. UCRL-ID-130811.
- Farmer, J.C.; McCright, R.D.; Estill, J.C.; and Gordon, S.R. 1999. *Proceedings of the Symposium on the Scientific Basis for Nuclear Waste Management XXII*, Fall Meeting of the Materials Research Society, Boston, Massachusetts.
- Farmer, J.C. 2000. *General Corrosion and Localized Corrosion of Waste Package Outer Barrier*, ANL-EBS-MD-000003 Rev. 0, CRWMS M&O, Las Vegas, NV.
- Gartland, P.O. 1997. Paper No. 417, *Corrosion* 97, NACE, Houston, TX.
- Gdowski, G.E. 1991. *Survey of Degradation Modes of Four Nickel-Chromium-Molybdenum Alloys*, UCRL-ID-108330, pp. 30–31, Tables 22–23.
- Gdowski, G.E. 1997a. *Formulation and Make-up of Simulated Dilute Water (SDW), Low Ionic Content Aqueous Solution*, Yucca Mountain Project, Lawrence Livermore National Laboratory, TIP-CM-06, Revision CN TIP-CM-06-0-2, Table 1, p. 3.
- Gdowski, G.E. 1997b. *Formulation and Make-up of Simulated Concentrated Water (SCW), High Ionic Content Aqueous Solution*, Yucca Mountain Project, Lawrence Livermore National Laboratory, TIP-CM-07, Revision CN TIP-CM-07-0-2, Table 1, pp. 3–4.
- Gdowski, G.E. 1997c. *Formulation and Make-up of Simulated Acidic Concentrated Water (SAW), High Ionic Content Aqueous Solution*, Yucca Mountain Project, Lawrence Livermore National Laboratory, TIP-CM-08, Revision CN TIP-CM-08-0-2, Table 1, p. 3.
- Gdowski, G.E. 2000. *Environment on the Surfaces of the Drip Shield and Waste Package Outer Barrier*, ANL-EBS-MD-000001 Rev. 0, Office of Civilian Radioactive Waste Management, Las Vegas, NV.
- Glass, R.S.; Overturf, G.E.; Van Konynenburg, R.A.; and McCright, R.D. 1986. *Corrosion Science* 26 8, 577–590.
- Gruss, K.A.; Cragolino, G.A.; Dunn, D.S.; and Sridar, N. 1998. Paper 149, *Corrosion* 98, NACE, Houston, TX.
- Hack, H.P. 1983. *Materials Performance* 22 6, 24–30.
- Harrar, J.E.; Carley, J.F.; Isherwood, W.F.; and Raber, E. 1990. UCID-21867, 111 p.
- Haynes International, 1988. Product Brochure H-2019C, Haynes International, Inc., Kokomo, IN, 22 p.
- Haynes International, 1987. Product Brochure H-2002B, Haynes International, Inc., Kokomo, IN, 15 p.
- Horn, J.A. 1999. *Approach and Supporting Data for MIC Modeling*, Lawrence Livermore National Laboratory, 13 p.
- Horn, J.A.; Rivera, A.; and Lian, T. 1998. Paper 152, *Corrosion* 98, NACE, Houston, TX.
- Kim, Y-K. 1987. *Journal of the Corrosion Science Society of Korea* 16 1, 25–30.
- Kim, Y-K. 1988. *Journal of the Corrosion Science Society of Korea* 17 1, 20–26.
- Kim, Y-K. 1999a. *Corrosion* 55 1, 81–88.
- Kim, Y-K. 1999b. Paper 437, *Corrosion* 99, NACE, Houston, TX.
- Leygraf, C. 1995. Chapter 12, *Corrosion Mechanisms in Theory and Practice*, P. Marcus, J. Oudar, Eds., Marcel Dekker, Inc., New York, NY.
- Lian, T.; Martin, S.; Jones, D.; Rivera, A.; and Horn, J. 1999. Paper No. 476, *Corrosion* 99, NACE, Houston, TX.
- Newman, J.S. 1991. Chapter 11, Section 11.5, *Electrochemical Systems*, 2nd Ed., Prentice Hall, Englewood Cliffs, NJ, pp. 250–251.
- Nystrom, E.A.; Lee, J.B.; Sagues, A.A.; and Pickering, H.W. 1994. *J. Electrochem. Soc.* 141 2, 358–361.
- Rebak R.B.; Koon, N.E.; Crook, P. 1999. *Proceedings of the 50th Meeting of the International Society of Electrochemistry*, Pavia, Italy, September 1999.
- Scully, J.R.; Hudson, J.L.; Lunt, T.; Ilevbare, G.; Kehler, B. 1999. Final Report, TRW/DOE YMP Purchase Order Number A10762JM8A, September 30, 1999, 27 p.
- Sedriks, A.J. 1996. *Corrosion of Stainless Steels*, Wiley-Interscience New York, NY, Table 5.2, 5.3, p. 179; p. 377, 9.12.
- Sridhar, N.; and Dunn, D.S. 1994. *Corrosion* 50 11, 857–872.
- Summers, T. 2000. *Aging and Phase Stability of Waste Package Outer Barrier*, ANL-EBS-MD-000002 Rev. 0, CRWMS M&O, Las Vegas, NV.
- Treseder, R.S.; Baboian, R.; Munger, C.G. editors, 1991. *NACE Corrosion Engineer's Reference Book*, 2nd, NACE, Houston, TX, pp. 156, 180.
- Walsh, D. W. 1989. Paper 187, *Corrosion* 99, NACE, Houston, TX.
- Walton, J.C.; Cragolino, G.S.; and Kalandros, K. 1996. *Corrosion Science* 38 1, 1–18.
- Wang, F. 1999. Memorandum, *Summary on the Modification of BSW Solutions for SCC Tests*, Lawrence Livermore National Laboratory.
- Weast, R.C. 1978. *Handbook of Chemistry and Physics*, 59th Ed., CRC Press, West Palm Beach, FL, p. B-161.
- Welsch, G.; Smialek, J.L.; Doychak, J.; Waldman, J.; and Jacobson, N.S. 1996. Chapter 2, *Oxidation and Corrosion of Intermetallic Alloys*, G. Welsch, P. D. Desai, Editors, CINDAS, Purdue University, West Lafayette, IN, pp. 121–266, 18.